On the Performance of Metamaterial based Printed Circuit Antenna for Blood Glucose Level Sensing Applications: A Case Study

Taha A. Elwi[1,2*], Hayder H. Al-Khaylani[3,4], Wasan S. Rasheed[5], Sana A. Al-Salim[6], Mohammed H. Khalil[7], Lubna Abbas Ali[8], Omar Almukhtar Tawfeeq[6], Saba T. Al-Hadeethi[7], Dhulfiqar Ali[1], Zainab S. Muqdad[8], Serkan Özbay[9], and Marwah. M. Ismael[10]

Abstract—**Due to the urgent need to develop technologies for continuous glucose monitoring in diabetes individuals, potential research has been applied by invoking the microwave techniques. Therefore, this work presents a novel technique based on a single port microwave circuit, antenna structure, based on Metamaterial (MTM) transmission line defected patch for sensing the blood glucose level in noninvasive process. For that, the proposed antenna is invoked to measure the blood glucose through the field leakages penetrated to the human blood through the skin. The proposed sensor is constructed from a closed loop connected to an interdigital capacitor to magnify the electric field fringing at the patch center. The proposed antenna sensor is found to operate excellently at the first mode, 0.6GHz, with S11 impedance matching less than -10dB. The proposed sensor performance is tested experimentally with 15 cases, different patients, through measuring the change in the S11 spectra after direct touching to the sensor a finger print of a patient. The proposed sensor is found to be effectively very efficient detector for blood glucose variation with a low manufacturing cost when printed on an FR-4 substrate. The experimental measurements are analyzed mathematically to obtain the calibration equation of the sensor from the curve fitting. Finally, the theoretical and the experimental results are found to be agreed very well with a percentage of error less than 10%.**

Index Terms—**Glucose, sensor, MTM, noninvasive.**

[1] International Applied and Theoretical Research Center (IATRC), Baghdad Quarter, Iraq, (e-mail: taelwi82@gmail.com)

[2] Islamic University Centre for Scientific Research, The Islamic University, Najaf, Iraq

[3] Laser and Optoelectronics Engineering Department, University of Technology, Baghdad, Iraq

[4] Computer Techniques Engineering, Al Hikma University College, Baghdad, Iraq

[5] Department of Information and Communications Engineering, Al-Khwarizmi College, University of Baghdad, Iraq

[6] Department of Mechatronics, Al-Khwarizmi College of Engineering, Baghdad University, Iraq

[7] Media Technology and Communication Engineering Department/College of Engineering, University of Information Technology and Communications, Baghdad, Iraq

[8] Electrical Engineering Department, College of Engineering, Mustansiriyah University, Baghdad, Iraq

[9] Electrical Electronics Engineering Department, Gaziantep University, Turkey

[10] Department of Information and Communication Engineering, College of Information Engineering, Al-Nahrain University, Baghdad, Iraq.

I. INTRODUCTION

Viktor Veselago first presented metamaterials (MTM) in 1967 [1]. Such structures may be called artificial materials with nontraditional properties [2]. These materials possess negative permittivity (ε) and negative permeability (μ) that in turn support the backward wave propagation of electromagnetic waves [3]. In 1999 an interesting subwavelength element realized as split ring resonator (SRR) to achieve negative permeability was proposed by Pendry [4]. Basically, SRR can be represented as tank of LC circuit possessing equivalent inductance (L) and the capacitance (C) between two concentric rings resonating at specific frequency [4]. The SRR has normally a size much less than, around wavelength (λ/10), the guided wavelength. Therefore, many researchers applied SRR as technique to retrieve the characterizations of materials [4].

In such process, the changes in the scattering parameters (S-parameters) with respect to a sample under test (SUT) introduction can be transferred through certain algorithm to retrieve the materials characterizations.

Microwave sensing is a reliable method for liquid characterization that has been employed in the past decade [5]. SRRs [6], complementary SRRs (CSRRs) [3], open CSRRs (OCSRRs) [4], closed ring resonator [5] and other miniaturized microwave resonators [6] based on transmission lines attracted a considerable attention of researchers for biomedical applications [6]. The electromagnetic properties of these structures depend on their operation frequency and quality factor changes with respect to different liquid introductions [7]. Through measuring S-parameters coefficients, complex dielectric parameters of SUT, the liquid characterizations can be addressed [8]. This has provided a new sensing platform for the biological, pharmaceutical, and fuel industries [9]. Most microwave biological sensors are mounted under ultra-thin cylindrical pipes [10] or slotted cylindrical tubes [11]. Based on measuring S-parameters magnitudes at certain frequency, materials under test losses can be extracted for quality detection [12]. Such technology, however, the resolution of high-losses was found a significant concern due to the issue of skin depth penetration [13]. On the other hand, most suggested methods require micro fluidic channel tubes to contain SUT; that add

DOI: 10.36244/ICJ.2024.1.7

extra losses and difficulty of penetrations [14]. Nevertheless, many sensors detection process is based on certain volume of SUT that limits their use for real-time monitoring applications [15]. Moreover, an additional size and fabrication cost could be ensure field retardation and phase change to analyze the dielectric characterization [17] in specific for biological solvent detection.

Based on the current development of microwave sensors technologies, fractal based MTM structures attracted researchers to realize effective and efficient sensors to achieve a high selectivity [18]. On top of that, MTM realizes excellent performance in the microwave ranges due to their nontraditional properties [19]. Moreover, MTM based fractal geometries use remain very excellent candidates in the biomedical aspects due to their size reduction in comparison to traditional microwave structures. For example, a MTM defected patch-based monopole antenna was presented in [20] for pollution detections. Authors in [21] proposed a study of using a traditional microstrip transmission line for liquid properties detection. Then, an extended study based on a fractal MTM structure was presented for blood glucose sensing using a microstrip transmission line loaded with carbon nanotube patch in [22]. The use of MTM patch-based nanoscale structures was introduced for gas detection in [23] and [24]. MTM based fractal structures were applied to realize as MTM defect on the ground plane for cancer cell detection based on their electrical properties' changes [25].

In this work, the proposed work is a design of a sensor antenna structure based on MTM inclusion for sensing applications. This paper, a new approach based on a single port antenna element via MTM transmission line structure is proposed for blood glucose level detection. The MTM is constructed from an interdigital capacitor structure with a closed loop ring. The proposed structure is designed for glucose detection. The paper is organized as follows: The geometrical details are discussed in section II. The analysis process and the parametric study are presented in section III. The experimental measurements are explained in section IV after conducting 15 cases for the proposed study. The paper is concluded in section V.

II. SENSOR DESIGN AND DETAILS

The proposed antenna is mounted on an FR-4 substrate of a dielectric constant ε_r=4.3 and loss tangent tanδ=0.025 with thickness h=1.6 mm. The copper metal is 35µm. The proposed antenna is compacted on 30×30 mm2 size. The antenna is fed with a 50Ω microstrip transmission line of 7.25mm width and extended to touch the patch at length of 1.5mm to be connected directly to the radiating structure. The proposed closed loop design details are shown in Fig1(a). The back panel is covered completely copper as appeared in Fig1(b).

In addition to the proposed closed loop in this design, a copper interdigital capacitor (C_{int}), see Fig1(c), is conducted to maximize the electrical field intensity [12] at the center of the patch where SUT would be positioned. All geometrical details of Fig1 are listed in Table 1.

III. MTM PATCH THEORETICAL ANALYSIS

As mentioned later, the proposed radiating patch consists of a closed loop coupled with C_{int}. Therefore, the proposed patch is structured in such way to provide maximum fringing from the C_{int} edges. The C_{int} unit cell is constructed as interfaced strip lines with an effective length (L_n) to provide the desirable resonant frequency (f_r). The resulted capacitance value of the used C_{int} can be calculated analytically from the following equation [26]:

$$C = \frac{\varepsilon_{re}\times10^{-3}}{18\pi}\frac{K(k)}{K'(k)}(n-1)\frac{L}{10^{-6}} \qquad (1)$$

where C is the capacitance in pF, ε_{re} is the effective relative permittivity, n is the capacitor figure number, L is the finger length, K and K' are elliptical integral coefficients and they are given as [27]:

$$K(k) = \int_0^{\frac{\pi}{2}}[1 - ksin(t)^2]^{-0.5}dt \qquad (2)$$

$$K'(k) = \int_0^{\frac{\pi}{2}}\left[1 - \left(\sqrt{1-k^2}\right)sin(t)^2\right]^{-0.5}dt \qquad (3)$$

where, k is the argument and can be calculated as [26]:

$$k = \left(tan\left(\frac{a\pi}{4b}\right)\right)^2 \qquad (4)$$

where:

$$a = \frac{W}{2} \text{ and } b = \frac{W+Z1}{2} \qquad (5)$$

where, W is the finger width and S is the separation distance between fingers.

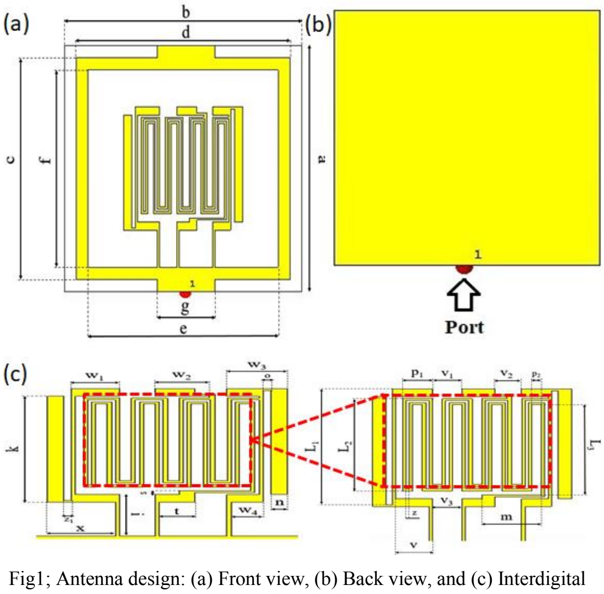

Fig1; Antenna design: (a) Front view, (b) Back view, and (c) Interdigital capacitor design.

TABLE I
GEOMETRICAL DETAILS OF THE PROPOSED ANTENNA SENSOR.

Parameter	Value (mm)	Parameter	Value (mm)
A	30	K	14
B	30	Z	0.25
C	27	Z_1	0.5
D	27	I	5.5
E	24	S	0.5
F	24	N	1
G	7.25	V_1	2.25
W_1	3	V_2	2
W_2	2.5	V_3	2.25
W_3	3.75	V	2.75
W_4	2	P_1	2.25
O	0.5	P_2	0.75
L_1	14.75	T	2.25
L_2	11.75	M	4.5
L_3	11.5	X	4.25

Now, the proposed sensor is analytically decomposed from the equivalent circuit diagram that is shown in Fig2. From Fig2, the proposed C_{int} is connected to two strip lines. The strip lines provide L-C branch (L_{strip} and C_{strip}) connection in parallel with C_{int}. OCSSR structure is connected to C_{int} through three shoring posts to be presented by (L_{short}) in the equivalent circuit diagram. It is good to mention that the effects of the inherent stray inductors (L_s) and stray capacitors (C_s) are proposed in the equivalent circuit diagram. Nevertheless, the feed line equivalently is considered as an inductor (L_{feed}). The equivalent representation for the closed loop (CL) is considered as an inductor (L_{CL}) and can be calculated according to the following equation [23]:

$$L = \mu_o a \left\{ ln\left(\frac{8a}{Z1}\right) - 2\right\} \tag{6}$$

Based on the circuit model in Fig2, the authors calculated the relative lumped elements with an initial gauss from equations (1 and 6) for the proposed design at the desired frequency band using ADS software package parametrically. The S-parameters are calculated from the circuit model to be shown in Fig. 2. It is found that the proposed sensor shows a resonance mode at 0.63GHz from the lumped elements that are listed in Table 2.

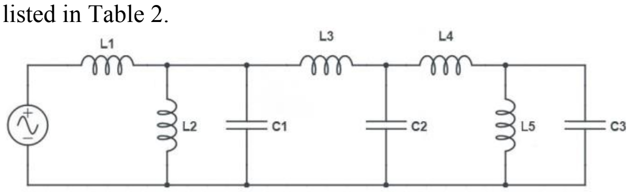

Fig2; Equivalent circuit for the proposed resonator.

TABLE II
CALCULATED LUMPED ELEMENTS

Lumped element	Value
L1	1.01nH
L2	1.89nH
L3	11.6mH
L4	23.04nH
L5	17.45nH
C1	11.12pF
C2	2.06pF
C3	1.91pF

From the proposed circuit model, the equivalent impedance is calculated based on the second branch to be described by L_2 and C_2 be noted as $Z_{T,2}$ following:

$$Z_{T,2} = \frac{j\omega L_2}{1-\omega^2 L_2 C_2} \tag{7}$$

Therefore, the resonant frequency, $f_{r,2}$ is expressed as

$$f_{r,2} = \frac{1}{2\pi\sqrt{L_2 C_2}} \tag{8}$$

In Fig. 2, the equivalent circuit of the proposed patch can be represented as two series of L_1C_c circuits and one parallel L_2C_2 circuit and the total impedance, $Z_{T,1}$ in addition to the band pass resonant frequency, $f_{r,1}$ which can be given as following:

$$Z_{T,1} = \frac{2(1-\omega^2 L_1 C_c)}{j\omega C_c} + \frac{j\omega L_2}{1-\omega^2 L_2 C_2} \tag{9}$$

$$f_{r,1} = \frac{1}{2\pi\sqrt{L_1 C_c}} \tag{10}$$

By employing (2) and (4), relation (3) can be rewritten as following:

$$Z_{T,1} = \frac{2(1-(\frac{\omega}{\omega_{r,1}})^2)}{j\omega C_c} + \frac{j\omega L_2}{1-(\frac{\omega}{\omega_{r,2}})^2} \tag{11}$$

$Z_{T,1}$ in relation (5) has two resonant frequencies, lower and upper frequencies which are represented by $\omega_{r,1}$ and $\omega_{r,2}$ respectively. When $\omega = \omega_{r,1}$ a maximum transmission could occur, where minimum $Z_{T,1}$ is ($Z_{T,1} \geq j\omega L_2$), while zero transmission occurs at $\omega = \omega_{r,2}$ where $Z_{T,1}$ maximum is achieved. In order to confirm prior discussion, an electromagnetic 3D simulation based on CST software packages in invoked to validate the obtained results from the circuit model. In Fig3, the patch is simulated when mounted in closed to a transmission line to evaluate the S_{11} spectrum. It is found that there are three resonant frequencies, $f_{r,1}$, $f_{r,2}$ and $f_{r,3}$, all these frequencies are the same resonant frequencies of the proposed patch. Therefore, these frequencies can be used as indicators for characterizing SUT after applying sensitivity analysis at the resonant frequencies.

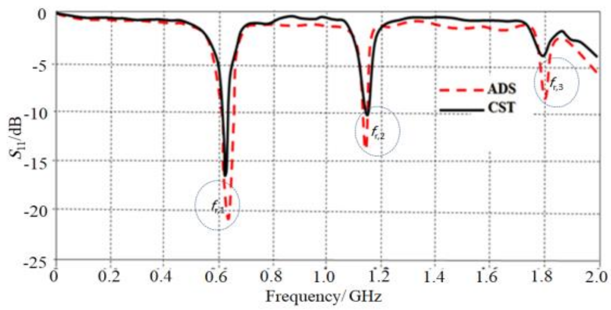

Fig 3; S_{11} spectra comparison between ADS and CST software packages.

IV. SENSITIVITY ANALYSIS

The proposed sensor is invented based on a quasi-static small antenna [12] in which designed with an interdigital capacitor surrounded with closed loop. Due to such combination a current circulation occurs at three legs of connection between the capacitor and the closed loop. The variation in the capacitance of the structure generally concerns on the variation in the permittivity of SUT. Therefore, the performance variation in the proposed structure with introducing different permittivity values is discussed as following:

A. Resonant frequencies analysis

After introducing different SUT in the CST MWS environment, the frequency shifts are recorded to be tested later experimentally. Therefore, SUT must cover the whole area for the efficient perturbation of the *E*-field. The resonant frequencies of S_{11} in Fig.4 are considered as the reference of unloaded filter ($f_{r,1}$ and $f_{r,2}$). The proposed sensor is then loaded with the SUT, where the dielectric constant of the sample is changed randomly in a broad range from 76 to 90. The resonant frequencies ($f_{r,1}$ and $f_{r,2}$) corresponding to each sample are extracted, which are also plotted with variation of the dielectric constant as shown in Fig. 4 (a). For preferable conception the change in the resonant frequencies (Δf_r= unloaded ($f_{r,1}$ and $f_{r,2}$) – corresponding loaded ($f_{r,1}$ and $f_{r,2}$)) is plotted in Fig. 4 (b).

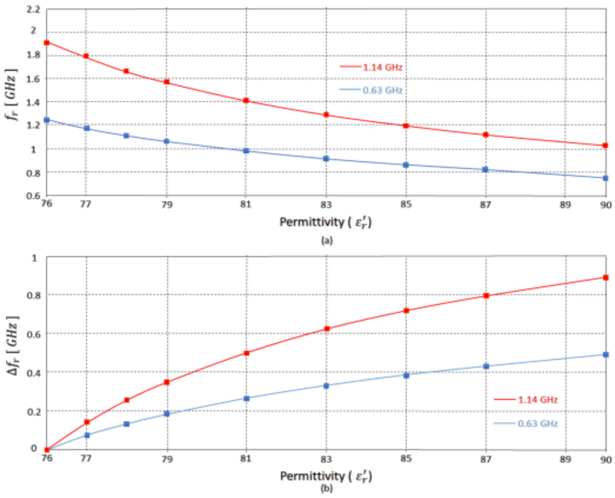

Fig. 4 Performance variation in terms of frequency resonance of the proposed sensor with changing ε_r: (a) f_r change and (b) Δf_r^{-1}.

From Fig. 4 (a) it can be noted that the resonant frequency, $f_{r,1}$ is about 170 MHz greater than resonant frequency, $f_{r,2}$. Moreover, the relative change $f_{r,1}$ with dielectric constant is about 150 MHz greater than $f_{r,2}$ as depicted in Fig. 4 (b). In another meaning, for these resonant frequencies, $f_{r,1}$ shows to be a good preference to obtain high sensitivity for supposed dielectric constant as compared to that of resonant frequency, $f_{r,1}$.

B. Quality factor analysis

For general resonators the quality factor, Q may be presented as [34]:

$$Q = \omega_o \frac{W}{P_L} \tag{12}$$

where, ω_0 is the angular resonant frequency, W is the electric and magnetic stored energy and P_L represents the average power dissipated per cycle. The previous equation also can be rewritten as:

$$Q = \frac{f_r}{\Delta f} \tag{13}$$

where f_r is the resonant frequency and Δf represents the relative 3dB bandwidth of the resonator frequency response. The proposed sensor performance is simulated with different values of loss tangent from 0.01 to 0.15 and corresponding ε'_r variation from 76 to 90. The relative quality factor is computed and depicted in Fig. 5.

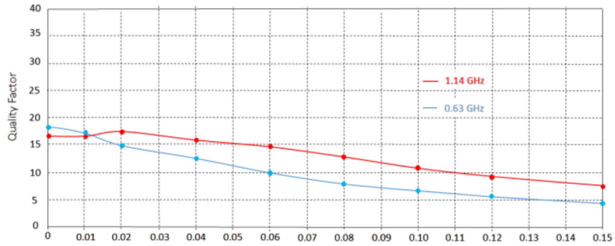

Fig. 5; Quality factor variation of the proposed sensor calculated for $f_{r,1}$ and $f_{r,2}$.

From Fig. 5, it is fully interesting to observe that the slope of quality factor is identical to resonant $f_{r,1}$ in comparison to $f_{r,2}$ slope with loss tangent change. While the slope of quality factor relative to $f_{r,1}$ is greater than in $f_{r,2}$ for the same condition. Hence the resonant $f_{r,1}$ is utilized for characterizing the SUT.

V. DATA ANALYSIS

Now, the obtained results from the previous section are analyzed to evaluate the calibration sensitivity to be compared to the experimental results. In order to describe the tested samples, a numerical type is desired which generally plots the measured parameters (e.g., the resonant frequency and the quality factor) to the relative permittivity of the SUT.

A. Real permittivity calibration effects

The proposed sensor frequency resonance is found to be changed due to samples loading as can be observed in Fig.6; in which the inverse square of the resonant frequency (f_r) is extracted from the S_{11} spectra. The results with the corresponding real permittivity (ε'_r) of SUT are depicted in Fig. 6.

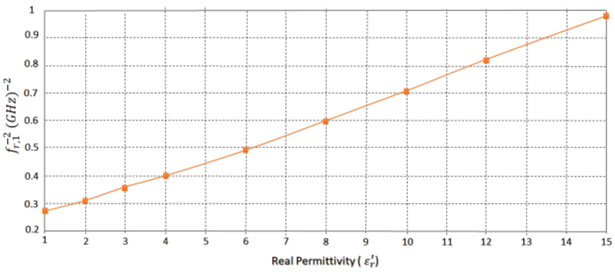

Fig. 6. $f^{-2}_{r,1}$ variation with respect of changing ε'_r.

The obtained results in Fig. 6 confirm the results in equation (10) that is achieved from the equivalent circuit model. From equation (10), the values of L_2 and C_2 are supposed to be constant due to the solid values of the overall length of OCSRRs and ε_r of the substrate. It is interesting to note that the inverse square of the resonant frequency is directly proportional to the real permittivity of the SUT. Thus, in order to combine all the above effects, the dielectric constant of the SUT is mathematically expressed in terms of the resonant frequency (f_r) as following:

$$\varepsilon_r' = -3.519(f_r^{-2})^2 + 23.84(f_r^{-2}) - 5.007 \tag{14}$$

The above relation is obtained from employing the curve fitting tools, which supplies a numerical model of the proposed sensor to determine the real permittivity of SUT in terms of the measured resonant frequency ($f_{r,1}$). It should be noted that all SUT has with a fixed 3mm thickness.

B. Imaginary permittivity calibration effects

After founding the numerical relations to determine the dielectric constant of SUT, an identical analysis is completed to find a numerical relation for computing the loss tangent (tanδ) of SUT. As explained earlier that the resonant $f_{r,1}$ provides a quality factor greater than those obtained at $f_{r,2}$. Hence, the resonant $f_{r,1}$ is employed for calculating tanδ of SUT. Therefore, at first, the dielectric constant in the range of 76 to 90 are possessed and the tanδ values combatable for each dielectric SUT is changed from 0 to 0.15, and the relative simulated results of $f_{r,1}$change is depicted in Fig. 7.

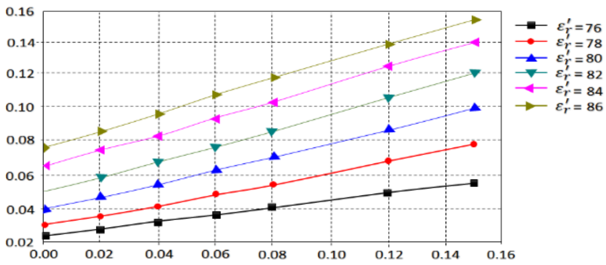

Fig. 7. Inverse of Q-factor in terms of tanδ for various values of ε'_r (Linear relevance between Q^{-1}_{SUT} and tanδ for all values of ε'_r).

The quality factor (Q_{SUT}) for each case is determined from the simulated response of S_{11}spectra, after that the inverse of Q_{SUT} values and the corresponding tanδ are depicted in Fig. 7. The relation between the tanδ and the Q_{SUT} can be specified as following [12]:

$$Q_{MUT} = \frac{1}{\tan\delta} = \frac{\varepsilon_r^{//}}{\varepsilon_r^{/}} \qquad (15)$$

where ε_r*'* and ε_r" are the real and imaginary parts of the relative permittivity in equation (15). From Fig. 7, it is noted that the alteration of Q^{-1}_{SUT} with tanδ is linear compound with a rising values depend on ε'_r of SUT. Thus, to deduce the tanδ of SUT, which relies on the loaded quality factor as well as the ε'_r of SUT, a curve fitting tool is utilized to conclude the numerical model as presented below:

$$\tan\delta = \exp\left(\frac{Q_{MUT}^{-1} + 0.02393}{0.2183 + 0.03131 \times \varepsilon_r}\right) - 1.16477 \quad (16)$$

After deciding the ε'_r from equation (14) and tanδ from (16), the imaginary part of the complex permittivity can be determined using (15).

VI. Sensor Fabrication

The proposed sensor is fabricated using printed circuit board technology as shown in Fig. 9. The sensor is fabricated from using chemical wit etching process in the laboratory. The FR4 substrate is considered as the plate form layer for the proposed sensor.

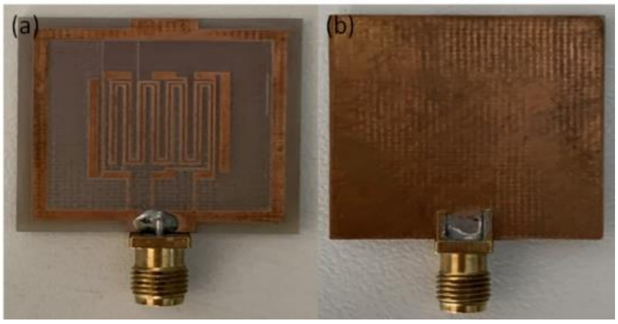

Fig. 8; Fabricated sensor structure: (a) front view and (b) back view.

Now, the proposed sensor performance is measured in terms of S_{11} spectrum as seen in Fig. 10 without introducing any SUT. The obtained results from measurements are compared to those obtained from simulation results to show excellent agreement as seen in Fig. 9.

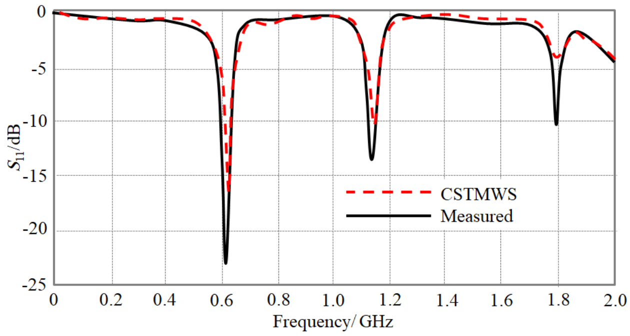

Fig 9; Experimental validation.

The measurement results are conducted to PNA8720 network analyzer after applying a single port calibration process. From the measured S_{11} spectra, the proposed sensor shows a frequency resonance at 0.63 GHz with $|S_{11}|$=16dB, and a bandwidth from 0.6GHz to 0.65GHz. This frequency is considered to ensure excellent penetration through the human tissues with minimum skin depth loss [6].

VII. Measurements and Validations

In this section, the proposed sensor measurement operation is based on placing a finger on the interdigital capacitor part to monitor the variation in the S_{11} magnitude and frequency resonance shift. The field penetration through the finger skin is affected by the blood glucose variation [12]. Such variation is attributed to the blood glucose change that could be reflected on the effective permittivity of the blood as discussed [23]. Therefore, the effects of touching the proposed sensor by 15 patients at three different times to realize 45 recorders are listed in Table 3 to analyze the sensor performance. The recorded data in Table 3 are collected based on S_{11} spectra change in terms of S_{11} magnitude, frequency resonance, phase change, bandwidth, and quality factor.

A. Sensing Process

The S_{11} spectra of the proposed sensor are obtained according to the samples listed in Table 3. The sensor is designed to ensure that the first resonant position is located around 0.63 GHz. Therefore, the fabricated sensor S_{11} spectra changes are evaluated after introducing the patient finger touch. Thus, the prepared design is experimentally tested using the PNA8720 network analyzer. The obtained changes in the S_{11} spectra are monitored in terms of $|S_{11}|$, frequency shift, phase change, quality factor, and bandwidth.

TABLE III
CLARIFICATION OF THE RESULTS OF MEASURING DIFFERENT BLOOD SAMPLES.

Case	BMI	Age	Sex	Glucose level	$f_{r,1}$ shift/ GHz	Q_{SUT}/ %	ε_r'	ε_r''
				112	0.1091	12	25.91	0.311
1	18.9	8	M	210	0.112	11	25.76	0.283
				150	0.115	11	25.59	0.281
				119	0.106	12	26.08	0.313
2	23.1	49	M	103	0.115	15	25.59	0.3833
				210	0.111	22	25.81	0.567
				250	0.123	9	25.16	0.226
3	22.9	65	F	225	0.193	8	21.59	0.172
				245	0.191	21	21.69	0.455
				131	0.103	31	26.25	0.813
4	27.8	50	F	159	0.109	9	25.92	0.233
				177	0.108	12	25.97	0.311
				331	0.121	11	25.27	0.278
5	26.5	59	F	193	0.111	13	25.81	0.335
				168	0.156	17	23.43	0.398
				102	0.116	15	25.54	0.383
6	29.9	38	F	131	0.182	10	22.13	0.221
				109	0.174	9	22.52	0.202
				158	0.091	16	26.9	0.43
7	30.2	44	M	146	0.098	13	26.52	0.344
				126	0.092	10	26.85	0.268
				110	0.109	11	25.92	0.282
8	28.5	43	M	191	0.106	12	26.08	0.313
				198	0.110	11	25.87	0.284
				104	0.122	7	25.22	0.176
9	24.1	48	F	107	0.133	7	24.63	0.172
				115	0.124	9	25.11	0.226
				119	0.111	11	25.81	0.283
10	32.6	41	F	131	0.110	13	25.87	0.336
				114	0.113	12	25.7	0.308
				121	0.091	10	26.9	0.269
11	36.1	53	M	180	0.094	7	26.74	0.187
				140	0.092	11	26.85	0.295
				390	0.109	9	25.92	0.233
12	32.6	67	F	331	0.101	7	26.36	0.184
				378	0.105	12	26.14	0.313
				190	0.189	11	21.79	0.239
13	22.4	61	F	143	0.188	10	21.83	0.218
				126	0.177	9	22.37	0.201
				129	0.109	12	25.92	0.311
14	23.5	62	M	130	0.110	11	25.87	0.284
				120	0.112	9	25.76	0.231
				121	0.195	4	21.5	0.086
15	24.9	54	M	189	0.196	5	21.45	0.107
				134	0.179	8	22.28	0.178

B. *Sensing Validation*

The variation in the S_{11} spectra of the proposed sensor is measured after placing a finger on it as a non-invasive technique. Therefore, the glucose level is monitored through a normal device glucose meter, PRODIGY Autocode, and the results are recorded in Table 3. Then, the patient finger is placed on the proposed sensor and the frequency resonance shift and S_{11} magnitude change are listed in Table 3. Next, the measured glucose level is compared with respect to the relative values of ε_r' and ε_r" that are listed in Table 3. Therefore, the measured $f_{r,1}$ and Q_{SUT} values are applied in equation (14) to (15) to calculate the relative values of ε_r' and ε_r" from the measured data. The calculated values of ε_r' and ε_r" are compared to their relatives from measurements in Table 3. Thus, in Table 4, the relative errors between the measured and calculated ε_r' and ε_r" values are calculated. It is found a good agreement between the measured and calculated values. Therefore, from this comparison between the relative values of ε_r' and ε_r", the glucose level can be detected according to Table 4.

TABLE IV
COMPARISON RELATIVE ERRORS BETWEEN THE MEASURED AND CALCULATED ε_R' AND ε_R" VALUES.

Case number	Measured values		Calculated values		Error rate for	Error rate for	Total error
	ε_r'	ε_r''	ε_r'	ε_r''	ε_r'	ε_r''	rate
	25.91	0.311	26.84	0.322	3.46%	3.41%	6.87%
1	25.76	0.283	25.87	0.284	0.42%	0.35%	0.77%
	25.59	0.281	26.52	0.291	3.5%	3.43%	6.93%
	26.08	0.313	27.01	0.324	3.44%	3.39%	6.83%
2	25.59	0.383	26.52	0.397	3.5%	3.52%	7.02%
	25.81	0.567	26.73	0.588	3.44%	3.57%	7.02%
	25.16	0.226	26.09	0.234	3.56%	3.41%	6.97%
3	21.59	0.172	22.51	0.180	4.08%	4.44%	8.52%
	21.69	0.455	22.61	0.474	4.06%	4%	8.06%
	26.25	0.813	27.17	0.842	3.38%	3.44%	6.82%
4	25.92	0.233	26.84	0.241	3.42%	3.31%	6.73%
	25.97	0.311	26.90	0.322	3.45%	3.41%	6.86%
	25.27	0.278	26.19	0.288	3.51%	3.47%	6.98%
5	25.81	0.335	26.73	0.347	3.44%	3.45%	6.89%
	23.43	0.398	24.36	0.414	3.81%	3.86%	7.67%
	25.54	0.383	26.46	0.396	3.47%	3.28%	6.75%
6	22.13	0.221	23.05	0.230	3.99%	3.91%	7.90%
	22.52	0.202	23.45	0.211	3.96%	4.26%	8.22%
	26.9	0.43	27.83	0.445	3.34%	3.37%	6.71%
7	26.52	0.344	27.44	0.356	3.35%	3.37%	6.72%
	26.85	0.268	27.77	0.277	3.31%	3.24%	6.55%
	25.92	0.285	26.84	0.295	3.46%	3.38%	6.84%
8	26.08	0.313	27.01	0.324	3.44%	3.39%	6.83%
	25.87	0.284	26.79	0.182	3.43%	56.04%	59.47%
	25.22	0.176	26.14	0.230	3.51%	23.47%	26.98%
9	24.63	0.172	25.56	0.234	3.63%	26.49%	30.12%
	25.11	0.226	26.03	0.294	3.53%	23.12%	26.65%
	25.81	0.283	26.73	0.348	3.44%	18.67%	22.11%
10	25.87	0.336	26.79	0.319	3.43%	5.32%	8.75%
	25.7	0.308	26.63	0.319	3.49%	3.44%	6.93%
	26.9	0.269	27.83	0.278	3.34%	3.23%	6.57%
11	26.74	0.187	27.66	0.193	3.32%	3.26%	6.58%
	26.85	0.295	27.77	0.305	3.31%	3.27%	6.58%
	25.92	0.233	26.84	0.241	3.42%	3.31%	6.73%
12	26.36	0.184	27.28	0.190	3.37%	3.15%	6.52%
	26.14	0.313	27.06	0.324	3.39%	3.39%	6.78%
	21.79	0.239	22.71	0.249	4.05%	4.01%	8.06%
13	21.83	0.218	22.76	0.227	4.08%	3.96%	8.04%
	22.37	0.201	23.30	0.209	3.99%	3.77%	7.76%
	25.92	0.311	26.84	0.322	3.42%	3.41%	6.83%
14	25.87	0.284	26.79	0.294	3.25%	3.40%	6.65%
	25.76	0.231	25.82	0.232	0.23%	0.43%	0.66%
	21.5	0.086	22.42	0.089	4.23%	3.37%	7.60%
15	21.45	0.107	22.37	0.111	4.11%	3.60%	7.71%
	22.28	0.178	23.20	0.185	3.96%	3.78%	7.74%
					Total error ratio for all measurements		9.76%

The total calculated error is evaluated from Table 4 according to the following equation:

$$\text{*error} = \frac{\| measured\ values - calculated\ values \|}{calculated\ values} \times 100 \qquad (17)$$

It is found the maximum error from the total values is less than 10%.

VIII. CONCLUSION

The proposed sensor is presented to characterize blood glucose level through measuring the relative values of ε_r' and ε_r" for different blood samples. The proposed sensor is constructed as a single-port network; therefore, it is designed based on an interdigital capacitor patch to sense the blood glucose level non-invasively. The reason of that, the field fringing from the proposed sensor is found to be magnified and easy to penetrate through the human skin to the blood vassals. It is found that the proposed sensor shows different frequency resonances within the band of interest. However, it is decided to consider only the first frequency resonance ($f_{r,1}$) for sensing where the maximum sensitivity can be achieved. In this case, $f_{r,1}$ and Q_{SUT} measurement are gathered from different patients. Therefore, from the measured values, an analytical model is synthesized based on curve fitting analysis. In such process, fifteen patients are submitted to the proposed sensor for estimating the level of glucose in the blood, ending with results very similar to the results measured by traditional commercial methods. The measured values of ε_r' and ε_r" are found to be agree very well with those obtained from the calculated results based on curve fitting analysis with less than 15% errors. It is found that the proposed sensor is a suitable choice for biomedical applications including blood glucose measurements. The proposed measurements point out the total error is about 10%. Finally, a future work on metamaterial-based printed circuit antennas for blood glucose level sensing applications includes optimizing antenna design, integrating with biosensors, miniaturization for wearable devices, ensuring biocompatibility, employing advanced signal processing techniques, conducting clinical validation, ensuring long-term stability, improving cost-effectiveness, and exploring multiparameter sensing capabilities. These efforts aim to enhance accuracy, reliability, and practicality for diabetes management and healthcare monitoring.

REFERENCES

[1] D. Whiting et al., "IDF diabetes atlas: global estimates of the prevalence of diabetes for 2011 and 2030". Diabetes Res. Clin. Pract. 94(3), 311–321 (2011). DOI: 10.1016/j.diabres.2011.10.029.

[2] "American Diabetes Association. Diagnosis and classification of diabetes mellitus". Diabetes Care 37, S81–S90 (2014). DOI: 10.2337/dc14-S081.

[3] "Pre diabetes diagnosis and treatment: a review". World J. Diabetes 6(2), 296-303 (2015). DOI: 10.4239/wjd.v6.i2.296.

[4] M. G. Burt et al., "Brief report: comparison of continuous glucose monitoring and finger-prick blood glucose levels in hospitalized patients administered basal-bolus insulin". Diabetes Technol. Ter. 15(3), 241–245 (2013). DOI: 10.1089/dia.2012.0282.

[5] W. V. Gonzales et al., "A progress of glucose monitoring - a review of invasive to minimally and non-invasive techniques, devices and sensors". Sensors 19(4), 800 (2019). DOI: 10.3390/s19040800.

[6] T. Lin et al., "Non-invasive glucose monitoring: a review of challenges and recent advances". Curr. Trends Biomed. Eng. Biosci. 6(5), 1–8 (2017). DOI: 10.19080/CTBEB.2017.06.555696.

[7] Spegazzini, N. et al. "Spectroscopic approach for dynamic bioanalyte tracking with minimal concentration information". Sci. Rep. 4, 7013 (2015). DOI: 10.1038/srep07013.

[8] Kuroda, M. et al. "Effects of daily glucose fluctuations on the healing response to everolimus-eluting stent implantation as assessed using continuous glucose monitoring and optical coherence tomography". Cardiovasc. Diabetol. 15(1), 79 (2016). DOI: 10.1186/s12933-016-0395-4.

[9] J. Y. Sim et al., "In vivo microscopic photoacoustic spectroscopy for non-invasive glucose monitoring invulnerable to skin secretion products". Sci. Rep. 8(1), 1059 (2018). DOI: 10.1038/s41598-018-19340-y.

[10] M. Goodarzi et al., "Selection of the most informative near infrared spectroscopy wavebands for continuous glucose monitoring in human serum". Talanta 146, 155–165 (2016). DOI: 10.1016/j.talanta.2015.08.033.

[11] J. Yadav et al., "Prospects and limitations of non-invasive blood glucose monitoring using near infrared spectroscopy". Biomed. Signal Process. Control 18, 214–227 (2015). DOI: 10.1016/j.bspc.2015.01.005.

[12] Y. Alnaiemy et al., "Electromagnetic Characterizations of Cement Using Free Space Technique for The Application of Buried Object Detection". Academic Science Journal, 2015, Volume 11, Issue 4, Pages 1 -10. DOI: 10.13140/RG.2.2.19212.56965.

[13] R. K. Abdulsattar et al., "A Theoretical Study to Design a Microwave Resonator for Sensing Applications". Journal of Engineering and Sustainable Development (JEASD), 2021, Volume, Issue Conference proceedings 2021, Pages 1-42-1-48. DOI: 10.31272/jeasd.conf.2.1.6.

[14] R. K. Abdulsattar et al., "Artificial Neural Network Approach for Estimation of Moisture Content in Crude Oil by Using a Microwave Sensor". International journal of microwave and optical technology, Vol.18, No.5, September 2023. DOI: 10.1016/j.diabres.2011.10.029.

[15] A. I. Anwer et al., "Minkowski Based Microwave Resonator for Material Detection over Sub-6 GHz 5G Spectrum," 2023 2nd International Conference on 6G Networking (6GNet), Paris, France, 2023, pp. 1-4. DOI: 10.1109/6GNet58894.2023.10317726.

[16] T. A. Elwi "Metamaterial based a printed monopole antenna for sensing applications". Int J RF Microw Comput Aided Eng. 2018; 28:e21470. DOI: 10.1002/mmce.21470.

[17] R. K. Abdulsattar et al., "A New Microwave Sensor Based on the Moore Fractal Structure to Detect Water Content in Crude Oil". Sensors 2021, 21, 7143. DOI: 10.3390/s21217143.

[18] A. A. Al-Behadili et al., "Differential Microstrip Sensor for Complex Permittivity Characterization of Organic Fluid Mixtures". Sensors 2021, 21, 7865. DOI: 10.3390/s21237865.

[19] A. I. Anwer et al., "A Fractal Minkowski Design for Microwave Sensing Applications". Journal of Engineering and Sustainable Development, 2022, 26(5), 78–83. DOI: 10.31272/jeasd.26.5.7.

[20] M. Alibakhshikenari et al., "Design of a Planar Sensor Based on Split-Ring Resonators for Non-Invasive Permittivity Measurement". Sensors. 2023; 23(11):5306. DOI: 10.3390/s23115306.

[21] R. K. Abdulsattar et al., "Optical-microwave sensor for real-time measurement of water contamination in oil derivatives", AEU - International Journal of Electronics and Communications, Volume 170, 2023. DOI: 10.1016/j.aeue.2023.154798.

[22] A. I. Anwer et al., "A theoretical study to design a microwave sensor for biomedical detections". AIP Conference Proceedings. Vol. 2787. No. 1. AIP Publishing, 2023. DOI: 10.1063/5.0148154.

[23] R. K. AbdulSattar et al., "Metamaterial Based Sensor Using Fractal Hilbert Structure for Liquid Characterization," 2023 International Conference on Electromagnetics in Advanced Applications (ICEAA), Venice, Italy, 2023, pp. 480-483. DOI: 10.1016/j.sbsr.2020.100395.

[24] T. A. Elwi et al., "A Passive Wireless Gas Sensor Based on Microstrip Antenna with Copper Nanorods," Progress In Electromagnetics Research B, Vol. 55, 347-364, 2013. DOI: 10.2528/PIERB13082002.

[25] Ali˙, D., et al., (2021). Metamaterial-based Printed Circuit Antenna for Biomedical Applications. Avrupa Bilim Ve Teknoloji Dergisi(26), 12-15.

[26] Saha, S. et al. "A glucose sensing system based on transmission measurements at millimetre waves using micro strip patch antennas". Sci. Rep. 7, 6855 (2017). DOI: 10.1038/s41598-017-06926-1.

[27] S. Mohan et al., "Wireless integration, design, modeling, and analysis of nanosensors, networks, and systems: a system engineering approach". Proceedings Volume 7291, Nanosensors, Biosensors, and Info-Tech Sensors and Systems; 72910G (2009). DOI: 10.1117/12.821554.

Taha A. Elwi received his B.Sc. in Electrical Engineering Department (2003) (Highest Graduation Award), and Postgraduate M.Sc. in Laser and Optoelectronics Engineering Department (2005) (Highest Graduation Award) from Al-Nahrain University Baghdad, Iraq. From April 2005 to August 2007, he worked with Huawei Technologies Company, in Baghdad, Iraq. On January 2008, he joined the University of Arkansas at Little Rock and he obtained his Ph.D. in December 2011 in system engineering and Science. He is considered of Stanford University's top 2% scientists in 2022. His research areas include wearable and implantable antennas for biomedical wireless systems, smart antennas, WiFi deployment, electromagnetic wave scattering by complex objects, design, modeling, and testing of metamaterial structures for microwave applications, design and analysis of microstrip antennas for mobile radio systems, precipitation effects on terrestrial and satellite frequency re-use communication systems, effects of the complex media on electromagnetic propagation and GPS. His research is conducted to consider wireless sensor networks based on microwave terminals and laser optoelectronic devices. The nano-scale structures in the entire electromagnetic spectrum are a part of his research interest. Also, his work is extended to realize advancements in reconfigurable intelligent surfaces and control the channel performance. Nevertheless, the evaluation of modern physics phenomena in wireless communication networks including cognitive radio networks and squint effects is currently part of his research. His research interests include pattern recognition, signal and image processing, machine learning, deep learning, game theory, and medical image analysis-based artificial intelligence algorithms and classifications. He serves as an editor in many international journals and publishers like, MDPI, IEEE, Springer, and Elsevier. He is currently the head of the International Applied and Theoretical Research Center (IATRC), Baghdad Quarter, Iraq. Also, he has been a member of the Iraqi scientific research consultant since 2016. He is leading three collaborations around the world regarding biomedical applications using microwave technology. He is the supervisor of many funded projects and Ph.D. theses with corresponding of more than 150 published papers and holding 10 patents.

Hayder H. Al-khaylani received B.Sc. degree in Electrical Engineering Department, Faculty of Engineering, from University of Baghdad, Iraq, 2007. M.Tec. Electronics and Communication Engineering Department from Sam Higginbottom University, India, 2012 and PhD. in Electrical and Computer Engineering Department, Faculty of Engineering, Altinbas University, Istanbul, Turkey. His research interests are in the areas of smart antennas and wearable systems.

Saba T. Al-Hadeethi was born in 1984 in Baghdad, Iraq. She received a BSc degree in electronics and communication Engineering in 2005 from AL-Nahrain University Engineering college, Baghdad. She obtained his MSc degree in Electronic and Communication Engineering in 2009 from the Department of Electronics and Communication Engineering from AL-Nahrain University in Baghdad and PhD. in Electrical and Computer Engineering Department, Faculty of Engineering, Altinbas University, Istanbul, Turkey. Her research interests are in the areas of antennas design for 5G applications.

Sana A. Nasser was born in 1988 in Baghdad, Iraq. She received a BSc degree in communication Engineering in 2015 from Al-Mamuan college, Baghdad. She obtained his MSc degree in Electronic and Communication Engineering from the Department of Electrical Engineering, University of Technology, in 2021. Currently, he is a lecturer in the department of Mechatronics Engineering, Alkawarizmi College, at University of Baghdad. Her fields of research are Artificial Neural Networks.

Omar Almukhtar T. Najm was born in 1990 in Baghdad, Iraq. He received a BSc degree in communication Engineering in 2011 from University of Baghdad, Baghdad, Iraq. He obtained his MSc degree in Electronic and Communication Engineering from the Department of Electronic and Communication Engineering, from University of Baghdad, Baghdad, Iraq, in 2015. His fields of research are Digital communication, STBC-MIMO and robotic control systems.

Zainab S. Muqdad received her B.Sc. degree in Electrical Engineering (2017) and her M. Sc. degree in Electronics and Communication Engineering (2022), both from the Mustansiriyah University, Baghdad, Iraq. Her research interests include antenna, microwave applications, microwave radiology imaging, neural network, metamaterials, biomedical wireless systems, and cancer detection.

Mohammed H. Khaleel received the B.Sc. degree in Electrical Engineering Department, Faculty of Engineering, from University of Baghdad, Iraq, 2007 and M.Tec. Electronics and Communication Engineering from Sam Higginbottom University, India, 2012 research interests are in the areas of wireless communication.

Wasan S. Rasheed was born in 1989 in Baghdad, Iraq. She received the B.Sc. degree in Communication Engineering in 2011 from University of Technology, Iraq. She obtains his MSc in Communication Engineering, from Electrical Engineering department, University of Technology, Iraq, 2013. Her current research interests are in the field of antennas design.